JOURNAL OF GUIDANCE, CONTROL, AND DYNAMICS
Vol. 25, No. 2, March–April 2002

Calibration of Measurement Delay in Global Positioning System/Strapdown Inertial Navigation System

Hyung Keun Lee* and Jang Gyu Lee†
Seoul National University, Seoul 151-742, Republic of Korea
and
Gyu-In Jee‡
Konkuk University, Seoul 143-701, Republic of Korea

The effect of a constant transmission delay that occurs in delivering measurements from a global positioning system receiver to a Kalman filter for an aided strapdown inertial navigation is analyzed. Steady-state conditions under the measurement delay are derived based on measurement residual observation. A new error model for circular trajectories is derived to show that the currently computed navigation variables converge not to the current true variables but to the neighborhood of the past true variables at the instant the delayed measurements were actually sampled. Based on the steady-state conditions and the new error model, causes and effects of an erroneously large estimation error of forward accelerometer bias are presented. To eliminate the undesirable delay effects given any combination of a global positioning system receiver and a strapdown inertial measurement unit, a simple delay calibration algorithm is proposed. The proposed algorithm is based on the characteristics that the heading error is biased by a controlled vehicle maneuver and advantageously requires no modification in onboard hardware.

Nomenclature

C = transformation matrix from b frame to n frame,

$$\begin{bmatrix} \cos\theta & -\sin\theta & 0 \\ \sin\theta & \cos\theta & 0 \\ 0 & 0 & 1 \end{bmatrix}$$

$\boldsymbol{f}$ = specific force vector expressed in n frame
g = magnitude of vertical gravity
$\boldsymbol{g}$ = gravity vector, $[0 \;\; 0 \;\; g]^T$
$\boldsymbol{n}_{\text{pos}}$ = global positioning system (GPS) position measurement noise vector
$\boldsymbol{n}_{\text{vel}}$ = GPS velocity measurement noise vector
$\boldsymbol{q}$ = quaternion representing a rotation from b frame to n frame, $[q_0 \;\; q_1 \;\; q_2 \;\; q_3]^T$
$\boldsymbol{r}$ = local position vector from starting point, $[r_N \;\; r_E \;\; r_D]^T$
$\boldsymbol{r}_{\text{GPS}}$ = GPS position solution vector

$$U = \begin{bmatrix} -q_1 & -q_2 & -q_3 \\ q_0 & -q_3 & q_2 \\ q_3 & q_0 & -q_1 \\ -q_2 & q_1 & q_0 \end{bmatrix}$$

$\boldsymbol{v}$ = Earth referenced velocity vector expressed in n frame, $[v_N \;\; v_E \;\; v_D]^T$
$\boldsymbol{v}_{\text{GPS}}$ = GPS velocity solution vector
v_m = speed

$$Y = \begin{bmatrix} -q_1 & -q_2 & -q_3 \\ q_0 & q_3 & -q_2 \\ -q_3 & q_0 & q_1 \\ q_2 & -q_1 & q_0 \end{bmatrix}$$

$\boldsymbol{z}_{\text{pos}}$ = indirect GPS position measurement vector
$\boldsymbol{z}_{\text{vel}}$ = indirect GPS velocity measurement vector
Δ = measurement delay
$\boldsymbol{\varepsilon}$ = gyro drift vector, $[\varepsilon_x \;\; \varepsilon_y \;\; \varepsilon_z]^T$
η_z = accumulated heading error correction
θ = heading angle
$\boldsymbol{\xi}$ = equivalent tilt angle expressed in b frame, $[\xi_x \;\; \xi_y \;\; \xi_z]^T$
$\boldsymbol{\rho}$ = transport rate vector (angular rate vector of n frame with respect to e frame expressed in n frame)
$\boldsymbol{\psi}$ = equivalent tilt angle expressed in c frame, $[\psi_N \;\; \psi_E \;\; \psi_D]^T$
$\boldsymbol{\Omega}$ = Earth rate vector expressed in n frame, $[\Omega_N \;\; 0 \;\; \Omega_D]^T$
$\boldsymbol{\omega}_{ij}^k$ = angular rate vector of j frame with respect to i frame expressed in k frame
$[\boldsymbol{\omega}_{ij}^k\times]$ = skew symmetric matrix that is constructed by $\boldsymbol{\omega}_{ij}^k$
ω_m = heading angular rate
$\boldsymbol{0}$ = zero vector or zero matrix of appropriate dimension
∇ = accelerometer bias vector, $[\nabla_x \;\; \nabla_y \;\; \nabla_z]^T$

Superscripts and Subscripts

b = true (virtual) body frame
b' = computed (virtual) body frame
c = computed navigation frame
e = Earth frame
i = inertial frame
n = true navigation frame
T = transpose

Special Symbols

$\|\bullet\|$ = norm
$|\bullet|$ = absolute value
$\equiv$ = definition
$:=$ = replacement

Received 29 December 2000; revision received 30 July 2001; accepted for publication 6 November 2001.

*Graduate Student, School of Electrical and Computer Engneering.
†Professor, School of Electrical and Computer Engneering. Senior Member AIAA.
‡Associate Professor, Department of Electronics Engneering.

I. Introduction

THE benefits of combining a global positioning system (GPS) receiver and a strapdown inertial measurement unit (IMU) are well known. In this hybrid configuration, the GPS receiver can provide various combinations of position-type and velocity-type measurements. As a result, the long-term stability of the strapdown inertial navigation system (SDINS) can be ensured by the GPS measurements, and the short-term faults of the GPS receiver can be effectively isolated by the SDINS. In spite of these benefits, there are practical difficulties in implementing the GPS/SDINS integrated navigation system. The fundamental problem is the difficulty in using the GPS measurements and the SDINS navigation variables in a perfectly time-synchronized manner. Among the various deterministic and stochastic components of the time-synchronization error, the most dominant term is the constant measurement delay that originates from the different processing priorities and communication cycles of the GPS receiver and the IMU. In this case, the GPS measurements are more likely to be delayed than the IMU data. For this reason, the time-synchronization error may also be referred to as the measurement delay.

The effects of the time-synchronization error on SDINS were first introduced by Bar-Itzhack and Vitek.[1] It was reported that an erroneous accelerometer bias may result if the time synchronization between the SDINS and the aiding sensor is not achieved. By formulation, it was shown that the false forward accelerometer bias and the delayed velocity measurement share the same mode of excitation. A covariance analysis was performed where the Kalman filter without measurement delay was used as a design model, and the Kalman filter with measurement delay was used as a truth model. By the covariance analysis result and additional validation by reprocessing the raw data, the measurement delay that was not modeled as an error state of the design model Kalman filter was shown to be the source of the large estimation error of the forward accelerometer bias.

Nowadays, time synchronization is one of the most important factors in designing various GPS/SDINS hybrid navigation systems. Several methods of achieving GPS/SDINS time synchronization were proposed such as provision of accurate pulse-per-second signal into IMU hardware or utilization of the IMU time tagging by both hardware and software.[2] Whatever method is applied, the time-synchronization error would exist, no matter how small it is, and nothing is reported in the literature regarding how accurate time synchronization should be to meet each specific navigational accuracy requirement. In addition, because more and more off-the-shelf IMUs and GPS receivers are available, a cheap and simple method of achieving time synchronization is desirable. We propose a method to compensate time discrepancies between GPS and SDINS measurements. The compensation is achieved by first identifying the measurement delay of GPS and then by modifying the input to GPS/SDINS Kalman filter.

This paper is organized as follows. In Sec. II, preliminary assumptions, a trajectory model, and a simplified error model will be explained. Based on the observation of the onboard measurement residual dynamics under the GPS measurement delay, useful steady-state conditions are derived. In Sec. III, a new error model, which is the key result of this study, is derived. The new error model provides an insight that all of the currently computed navigation variables on the circular trajectories converge not to current true variables but to the neighborhood of the past true variables at the instant the delayed GPS measurements were actually sampled. In Sec. IV, an analysis is performed on the causes and effects of an erroneously large estimation error of the forward accelerometer bias, which is one of the most representative phenomena in the presence of the measurement delay. It will be shown that a biased heading error, together with an abrupt change of the steady-state conditions, is the key element that stimulates a large false forward accelerometer bias during S turns. In Sec. V, a simple delay calibration algorithm based on a controlled vehicle maneuver is proposed. The proposed algorithm enables identification and removal of the constant measurement delay for any GPS and IMU integration. Simulation and experimental results are presented to show the performance of the proposed algorithm. In Sec. VI, conclusions are given.

II. Error with Respect to Current Time

A. Assumptions and Trajectory

For brevity of derivations and identification of major characteristics, we will use the following assumptions throughout the analysis.

Assumption 1: A measurement delay Δ is assumed constant, and both the position and velocity errors due to Δ can be expanded to only a quadratic in Δ with a negligible error.

Assumption 2: A velocity $\boldsymbol{v}$ of a vehicle is assumed small enough so that the resulting transport rate $\boldsymbol{\rho}$ is negligible as compared with the Earth rate $\boldsymbol{\Omega}$:

$$\|\boldsymbol{\rho}\| \ll \|\boldsymbol{\Omega}\| \tag{1}$$

Assumption 3: A local position $\boldsymbol{r}$ from a starting point is assumed small so that the cross product $\boldsymbol{\rho} \times \boldsymbol{r}$ is negligible compared with the velocity $\boldsymbol{v}$:

$$\|\boldsymbol{\rho} \times \boldsymbol{r}\| \ll \|\boldsymbol{v}\| \tag{2}$$

Assumption 4: A constant angular rate ω_m of a circular trajectory satisfies

$$|\omega_m| \gg \|2\boldsymbol{\Omega}\| \tag{3}$$

Assumption 5: A local gravity vector $\boldsymbol{g}$ is assumed constant, and its error is assumed negligible.

Assumption 6: GPS position and velocity solutions caused by error sources other than the measurement delay Δ are not biased at each epoch.

Assumption 7: The inertial sensor errors contain only constant bias terms.

Assumption 8: Products of errors are negligible.

The constant measurement delay that is considered in this study originates from different processing and communication cycles of GPS measurements and IMU data. Thus, it does not change significantly once each subsystem is turned on. Assumptions 2 and 3 mean that the vehicle of interest moves only within a local area of the Earth with a moderate speed. This condition is met by various low-speed air vehicles and land vehicles. Assumption 6 means that both the position and velocity solutions provided by a GPS receiver are not biased if no delay exists.

Throughout this paper, we consider only the following circular trajectory model that may constitute the segments of a representative in-flight alignment. A straight flight trajectory with a constant velocity can be represented by setting $\omega_m = 0$. Various types of trajectories can also be approximated by successive combinations of circular trajectory segments. The circular trajectory model is

$$\dot{\theta}(t) = \omega_m \tag{4}$$

$$C = \begin{bmatrix} \cos\theta(t) & -\sin\theta(t) & 0 \\ \sin\theta(t) & \cos\theta(t) & 0 \\ 0 & 0 & 1 \end{bmatrix} \tag{5}$$

$$\boldsymbol{v}(t) = [v_m \cos\theta(t) \quad v_m \sin\theta(t) \quad 0]^T \tag{6}$$

$$\dot{\boldsymbol{v}}(t) = [-v_m\omega_m \sin\theta(t) \quad v_m\omega_m \cos\theta(t) \quad 0]^T \tag{7}$$

$$\boldsymbol{f} = \{0 \quad v_m(\omega_m + 2\Omega_D) \quad -[g - 2v_m\Omega_N \sin\theta(t)]\}^T \tag{8}$$

$$\boldsymbol{\omega}_{nb}^b = [0 \quad 0 \quad \omega_m]^T \tag{9}$$

$$\boldsymbol{\omega}_{ib}^b = \boldsymbol{\omega}_{ie}^b + \boldsymbol{\omega}_{nb}^b = [\Omega_N \cos\theta(t) \quad \Omega_N \sin\theta(t) \quad \Omega_D + \omega_m]^T \tag{10}$$

In Eqs. (4–10), ω_m, v_m, and $\boldsymbol{\omega}_{nb}^b$ are constant variables. Note that the effects of the transport rate $\boldsymbol{\rho}$ in Eqs. (8) and (10) are neglected by virtue of Assumption 2. As shown in Eqs. (5–8) and (10), the time arguments are selectively used if necessary.

B. Error Model with Respect to Current Time

By the assumptions explained in the preceding section, the basic SDINS navigation equations for the position $\boldsymbol{r}$, the velocity $\boldsymbol{v}$, the

quaternion $\boldsymbol{q}$, and the coordinate transformation matrix C can be simply written as[3]

$$\dot{\boldsymbol{r}} = \boldsymbol{v} \tag{11}$$

$$\dot{\boldsymbol{v}} = C\boldsymbol{f} - 2\boldsymbol{\Omega} \times \boldsymbol{v} + \boldsymbol{g} \tag{12}$$

$$\dot{\boldsymbol{q}} = \tfrac{1}{2}U\boldsymbol{\omega}_{ib}^{b} - \tfrac{1}{2}Y\boldsymbol{\omega}_{in}^{n} \tag{13}$$

$$C = C_b^n = Y^T U \tag{14}$$

Note that Assumption 3 is used in Eq. (11) and that Eq. (12) is a result of Assumption 2. The b frame appearing in the preceding mechanization equations represents the virtual body frame whose x axis points horizontally forward (along track), y axis points horizontally to the right (cross track), and z axis is in the direction of the local vertical. The b frame can also be obtained by eliminating both the roll and pitch angles of the physical body frame. For the implementation of Eqs. (11–14), we actually perform the following computations using the estimated and measured variables:

$$\dot{\hat{\boldsymbol{r}}} = \hat{\boldsymbol{v}} \tag{15}$$

$$\dot{\hat{\boldsymbol{v}}} = \hat{C}\bar{\boldsymbol{f}} - 2\hat{\boldsymbol{\Omega}} \times \hat{\boldsymbol{v}} + \hat{\boldsymbol{g}} \tag{16}$$

$$\dot{\hat{\boldsymbol{q}}} = \tfrac{1}{2}\hat{U}\bar{\boldsymbol{\omega}}_{ib}^{b} - \tfrac{1}{2}\hat{Y}\hat{\boldsymbol{\omega}}_{in}^{n} \tag{17}$$

$$\hat{C} = \hat{Y}^T \hat{U} \tag{18}$$

where the carets denote an estimated variable and the overbar denotes a measured variable. In expressing inertial navigation system errors, either the n frame or the c frame[3–6] can be used as a reference frame. As compared with the n frame that represents a locally level frame whose origin is located at the true position of a vehicle, the c frame represents the locally level frame that corresponds to the estimated position of the vehicle. The difference between the n frame and the c frame originates from the position error of the vehicle. This paper deals with the cases where the position error can be bounded by GPS position solutions. Though GPS position solutions are affected by a time-synchronization error, because the resultant position error is negligibly small compared to the local radii of curvature of the Earth, there is no significant difference between the n frame and the c frame. When the c frame is used as the reference frame, the error variables with respect to a current time t are defined as

$$\delta\boldsymbol{r}(t) \equiv \hat{\boldsymbol{r}}(t) - \boldsymbol{r}(t) \tag{19}$$

$$\delta\boldsymbol{v}(t) \equiv \hat{\boldsymbol{v}}(t) - \boldsymbol{v}(t) \tag{20}$$

$$\delta\boldsymbol{q}(t) \equiv \hat{\boldsymbol{q}}(t) - \boldsymbol{q}(t) \tag{21}$$

$$\boldsymbol{\psi}(t) \equiv -2\hat{Y}(t)^T \delta\boldsymbol{q}(t) \tag{22}$$

$$\nabla(t) \equiv \bar{\boldsymbol{f}}(t) - \boldsymbol{f}(t) \tag{23}$$

$$\boldsymbol{\varepsilon}(t) \equiv \bar{\boldsymbol{\omega}}_{ib}^{b}(t) - \boldsymbol{\omega}_{ib}^{b}(t) \tag{24}$$

where the 3×1 vector $\boldsymbol{\psi}(t)$ indicates an attitude error expressed in the c frame.[3] If we follow the procedure similar to Ref. 3 using Eqs. (11–24), the following simplified error model can be derived:

$$\delta\dot{\boldsymbol{r}} = \delta\boldsymbol{v} \tag{25}$$

$$\delta\dot{\boldsymbol{v}} = -2\boldsymbol{\Omega} \times \delta\boldsymbol{v} + (C\boldsymbol{f}) \times \boldsymbol{\psi} + C\nabla \tag{26}$$

$$\dot{\boldsymbol{\psi}} = -\boldsymbol{\omega}_{in}^{n} \times \boldsymbol{\psi} - C\boldsymbol{\varepsilon} \tag{27}$$

$$\dot{\nabla} = \boldsymbol{0} \tag{28}$$

$$\dot{\boldsymbol{\varepsilon}} = \boldsymbol{0} \tag{29}$$

In Eqs. (28) and (29), Assumption 7 is employed. To express SDINS attitude error, we can use an equivalent tilt angle $\boldsymbol{\xi}$ with respect to the b frame instead of the equivalent tilt angle $\boldsymbol{\psi}$ with respect to the c frame.[3] Thus, Eqs. (22), (26), and (27) are equivalent to the following error equations, respectively:

$$\boldsymbol{\xi}(t) \equiv -2\hat{U}(t)^T \delta\boldsymbol{q}(t) = C(t)^T \boldsymbol{\psi}(t) \tag{30}$$

$$\delta\dot{\boldsymbol{v}} = -2\boldsymbol{\Omega} \times \delta\boldsymbol{v} + C(\boldsymbol{f} \times \boldsymbol{\xi}) + C\nabla \tag{31}$$

$$\dot{\boldsymbol{\xi}} = -\boldsymbol{\omega}_{ib}^{b} \times \boldsymbol{\xi} - \boldsymbol{\varepsilon} \tag{32}$$

The physical meaning of $\boldsymbol{\xi}$ can be expressed as

$$C_{b(t)}^{b'(t)} = \boldsymbol{I} + [\boldsymbol{\xi}(t)\times] \tag{33}$$

where $\boldsymbol{b}(t)$ frame indicates the true body frame at t, $\boldsymbol{b}'(t)$ frame indicates the computed body frame at t, and $[\boldsymbol{\xi}(t)\times]$ indicates the 3×3 skew symmetric matrix that is constructed by $\boldsymbol{\xi}(t)$.

C. Steady-State Conditions

To bound the Kalman filter error states, either position-type GPS measurements or velocity-type GPS measurements can be used. Indirect measurement equations by delayed GPS data are modeled as follows[1]:

$$z_{\text{vel}}(t) = \hat{\boldsymbol{v}}(t) - \boldsymbol{v}_{\text{GPS}}(t) = \hat{\boldsymbol{v}}(t) - [\boldsymbol{v}(t-\Delta) + \boldsymbol{n}_{\text{vel}}(t-\Delta)] \tag{34}$$

$$z_{\text{pos}}(t) = \hat{\boldsymbol{r}}(t) - \boldsymbol{r}_{\text{GPS}}(t) = \hat{\boldsymbol{r}}(t) - \lfloor \boldsymbol{r}(t-\Delta) + \boldsymbol{n}_{\text{pos}}(t-\Delta) \rfloor \tag{35}$$

By Assumptions 1 and 3, $\boldsymbol{r}(t-\Delta)$ and $\boldsymbol{v}(t-\Delta)$ on a circular trajectory are expressed as follows:

$$\boldsymbol{v}(t-\Delta) = \boldsymbol{v}(t) - \dot{\boldsymbol{v}}(t)\Delta + \tfrac{1}{2}\ddot{\boldsymbol{v}}(t)\Delta^2 \tag{36}$$

$$\boldsymbol{r}(t-\Delta) = \boldsymbol{r}(t) - \boldsymbol{v}(t)\Delta + \tfrac{1}{2}\dot{\boldsymbol{v}}(t)\Delta^2 \tag{37}$$

Combining Eqs. (34–37), we obtain

$$z_{\text{vel}}(t) = \delta\boldsymbol{v}(t) + \dot{\boldsymbol{v}}(t)\Delta - \tfrac{1}{2}\ddot{\boldsymbol{v}}(t)\Delta^2 - \boldsymbol{n}_{\text{vel}}(t-\Delta) \tag{38}$$

$$z_{\text{pos}}(t) = \delta\boldsymbol{r} + \boldsymbol{v}\Delta - \tfrac{1}{2}\dot{\boldsymbol{v}}\Delta^2 - \boldsymbol{n}_{\text{pos}}(t-\Delta) \tag{39}$$

The Kalman filter drives the expectations of the measurement residuals to zero by achieving internal steady-state conditions. Thus, as the Kalman filter approaches a steady state, the following are observed:

$$\begin{bmatrix} \hat{z}_{\text{vel}} \\ \dot{\hat{z}}_{\text{vel}} \\ \ddot{\hat{z}}_{\text{vel}} \\ \vdots \end{bmatrix} \to \begin{bmatrix} \boldsymbol{0} \\ \boldsymbol{0} \\ \boldsymbol{0} \\ \vdots \end{bmatrix}, \qquad \begin{bmatrix} \hat{z}_{\text{pos}} \\ \dot{\hat{z}}_{\text{pos}} \\ \ddot{\hat{z}}_{\text{pos}} \\ \vdots \end{bmatrix} \to \begin{bmatrix} \boldsymbol{0} \\ \boldsymbol{0} \\ \boldsymbol{0} \\ \vdots \end{bmatrix} \tag{40}$$

$$\dot{\hat{z}}_{\text{pos}} = \hat{z}_{\text{vel}} \tag{41}$$

$$\hat{z}_{\text{vel}} \equiv \boldsymbol{E}[z_{\text{vel}}], \qquad \hat{z}_{\text{pos}} \equiv \boldsymbol{E}\lfloor z_{\text{pos}} \rfloor \tag{42}$$

If sufficient time has passed after the velocity-aided Kalman filter entered into the steady state, we can establish the following steady state conditions according to Eqs. (38–42):

$$\delta\boldsymbol{v} = -\dot{\boldsymbol{v}}\Delta + \tfrac{1}{2}\ddot{\boldsymbol{v}}\Delta^2 \tag{43}$$

$$\delta\dot{\boldsymbol{v}} = -\ddot{\boldsymbol{v}}\Delta + \tfrac{1}{2}\dddot{\boldsymbol{v}}\Delta^2 \tag{44}$$

If we use a position-aided Kalman filter, the following condition should hold according to Eqs. (39) and (40),

$$\delta\boldsymbol{r} = -\boldsymbol{v}\Delta + \tfrac{1}{2}\dot{\boldsymbol{v}}\Delta^2 \tag{45}$$

When Eqs. (31), (43), and (44) are combined, the following relationship is established with respect to the b frame:

$$\boldsymbol{f} \times \boldsymbol{\xi} + \nabla = -C^T\{\ddot{\boldsymbol{v}} + 2(\boldsymbol{\Omega} \times \dot{\boldsymbol{v}})\}\Delta + C^T\left\{\tfrac{1}{2}\dddot{\boldsymbol{v}} + (\boldsymbol{\Omega} \times \ddot{\boldsymbol{v}})\right\}\Delta^2 \tag{46}$$

By Eqs. (5–7), the following conditions also hold on a circular trajectory segment:

$$C^T\ddot{\boldsymbol{v}} = \begin{bmatrix} -v_m\omega_m^2 \\ 0 \\ 0 \end{bmatrix}, \qquad C^T\dddot{\boldsymbol{v}} = \begin{bmatrix} 0 \\ -v_m\omega_m^3 \\ 0 \end{bmatrix} \tag{47}$$

$$C^T(\boldsymbol{\Omega}\times\dot{\boldsymbol{v}}) = \begin{bmatrix} -v_m\omega_m\Omega_D \\ 0 \\ v_m\omega_m\Omega_N\cos\theta(t) \end{bmatrix}$$

$$C^T(\boldsymbol{\Omega}\times\ddot{\boldsymbol{v}}) = \begin{bmatrix} 0 \\ -v_m\omega_m^2\Omega_D \\ -v_m\omega_m^2\Omega_N\sin\theta(t) \end{bmatrix} \tag{48}$$

Substituting Eqs. (8), (47), and (48) into Eq. (46), we obtain the following steady-state conditions under a constant measurement delay Δ:

$$\nabla_x + [g - 2v_m\Omega_N\sin\theta(t)]\xi_y + v_m\omega_m\xi_z = v_m\omega_m^2\Delta + 2v_m\omega_m\Omega_D\Delta \tag{49}$$

$$\nabla_y - [g - 2v_m\Omega_N\sin\theta(t)]\xi_x = -v_m\omega_m^3\Delta^2/2 - v_m\omega_m^2\Omega_D\Delta^2 \tag{50}$$

$$\nabla_z - v_m\omega_m\xi_x = -2v_m\omega_m\Omega_N\Delta\cos\theta(t) - v_m\omega_m^2\Omega_N\Delta^2\sin\theta(t) \tag{51}$$

The right sides of the preceding equations are the driving terms caused by the measurement delay Δ on a circular trajectory segment. By Assumption 4, the effects of $2v_m\omega_m\Omega_D\Delta$ in Eq. (49) and $v_m\omega_m^2\Omega_D\Delta^2$ in Eq. (50) can be neglected.

III. Error with Respect to Past Time

In this section, by presenting a new error model that is applicable to a circular trajectory, we will show that the computed navigation variables converge not to the true variables but to the neighborhood of the past true variables at the instant when the delayed GPS measurements were actually sampled. For this purpose, we establish the new error definitions as follows. The newly defined error states are closely related to the measurement delay,

$$\delta\tilde{\boldsymbol{v}}(t) \equiv \hat{\boldsymbol{v}}(t) - \boldsymbol{v}(t-\Delta) \tag{52}$$

$$\delta\tilde{\boldsymbol{q}}(t) \equiv \boldsymbol{q}(t) - \boldsymbol{q}(t-\Delta) \tag{53}$$

$$\tilde{\boldsymbol{\xi}}(t) \equiv -2\hat{U}(t)^T\delta\tilde{\boldsymbol{q}}(t-\Delta) \tag{54}$$

$$\tilde{\nabla}(t) \equiv \bar{\boldsymbol{f}}(t) - \boldsymbol{f}(t) + \boldsymbol{b}_\nabla \tag{55}$$

$$\boldsymbol{b}_\nabla \equiv C^T\left[\tfrac{1}{2}\dddot{\boldsymbol{v}} + (\boldsymbol{\Omega}\times\ddot{\boldsymbol{v}}) - \tfrac{1}{2}C\ddot{\boldsymbol{f}}\right]\Delta^2 = \begin{bmatrix} 0 \\ -v_m\omega_m^2\left(\frac{1}{2}\omega_m + \Omega_D\right)\Delta^2 \\ 0 \end{bmatrix} \tag{56}$$

$$\tilde{\varepsilon}(t) \equiv \bar{\boldsymbol{\omega}}_{ib}^b(t) - \boldsymbol{\omega}_{ib}^b(t) \tag{57}$$

In Eqs. (52–54), the time-domain arguments for the true variables are used to clarify the differences from the conventional error definitions of Eqs. (20), (21), and (30), respectively. In Eq. (56), $\boldsymbol{b}_\nabla$ is the constant equivalent accelerometer bias vector that is generated by the measurement delay Δ while traveling on a circular trajectory. As compared with the definition of the accelerometer bias $\tilde{\nabla}$, the definition of the gyro drift $\tilde{\varepsilon}$ is unaltered because it will simplify the interpretation of the new error model.

From Eqs. (20), (36), and (52), the conventional velocity error $\delta\boldsymbol{v}(t)$ and the newly defined velocity error $\delta\tilde{\boldsymbol{v}}(t)$ satisfy the following relationship:

$$\delta\tilde{\boldsymbol{v}}(t) = \delta\boldsymbol{v}(t) + \dot{\boldsymbol{v}}\Delta + \tfrac{1}{2}\ddot{\boldsymbol{v}}\Delta^2 \tag{58}$$

Based on the definition of the velocity error $\delta\tilde{\boldsymbol{v}}(t)$, the onboard measurement equation can be rewritten as

$$\boldsymbol{z}_{\text{vel}}(t) = \delta\tilde{\boldsymbol{v}}(t) + \boldsymbol{n}_{\text{vel}}(t-\Delta) \tag{59}$$

If GPS/SDINS Kalman filter does not account for the existence of the measurement delay Δ in $\boldsymbol{z}_{\text{vel}}(t)$, it detects $\delta\tilde{\boldsymbol{v}}(t)$ rather than $\delta\boldsymbol{v}(t)$. It will be shown later that the appearance of the newly defined error model of $\delta\tilde{\boldsymbol{v}}$, $\tilde{\boldsymbol{\xi}}$, $\tilde{\nabla}$, and $\tilde{\varepsilon}$ is the same as the appearance of the conventional error model of $\delta\boldsymbol{v}$, $\boldsymbol{\xi}$, ∇, and ε except for small equivalent inertial sensor disturbances. Thus, the GPS/SDINS Kalman filter, ignoring the measurement delay Δ, actually tends to estimate $\delta\tilde{\boldsymbol{v}}$, $\tilde{\boldsymbol{\xi}}$, $\tilde{\nabla}$, and $\tilde{\varepsilon}$ rather than $\delta\boldsymbol{v}$, $\boldsymbol{\xi}$, ∇, and ε.

By Eqs. (21) and (53), the newly defined quaternion error $\delta\tilde{\boldsymbol{q}}(t)$ and the conventional quaternion error $\delta\boldsymbol{q}(t)$ satisfy the following relationship:

$$\begin{aligned}\delta\tilde{\boldsymbol{q}}(t) &= [\hat{\boldsymbol{q}}(t) - \boldsymbol{q}(t)] + [\boldsymbol{q}(t) - \boldsymbol{q}(t-\Delta)] \\ &= \delta\boldsymbol{q}(t) + \dot{\boldsymbol{q}}(t)\Delta + \tfrac{1}{2}\ddot{\boldsymbol{q}}(t)\Delta^2\end{aligned} \tag{60}$$

Compared with the conventional quaternion error $\delta\boldsymbol{q}(t)$ that is related to $\delta\boldsymbol{v}(t)$, the newly defined quaternion error $\delta\tilde{\boldsymbol{q}}(t)$ is related to $\delta\tilde{\boldsymbol{v}}(t)$. To derive the relationship between the conventional equivalent tilt angle $\boldsymbol{\xi}(t)$ and the newly defined equivalent tilt angle $\tilde{\boldsymbol{\xi}}(t)$, several preliminaries are required. At first, it can be easily shown that the quaternion differential equation of Eq. (13) is equivalent to the following differential equations:

$$\dot{\boldsymbol{q}}(t) = \frac{1}{2}U(t)\boldsymbol{\omega}_{nb}^b = \frac{1}{2}W\boldsymbol{q}(t), \qquad W \equiv \left[\begin{array}{c|c} 0 & -\left(\boldsymbol{\omega}_{nb}^b\right)^T \\ \hline \boldsymbol{\omega}_{nb}^b & -\left[\boldsymbol{\omega}_{nb}^b\times\right] \end{array}\right] \tag{61}$$

where $\boldsymbol{\omega}_{nb}^b$ and W are constant on the circular trajectories. Differentiating Eq. (61), we obtain the following equations:

$$\ddot{\boldsymbol{q}}(t) = \tfrac{1}{2}\dot{U}(t)\boldsymbol{\omega}_{nb}^b = \tfrac{1}{2}W\dot{\boldsymbol{q}}(t) = \tfrac{1}{4}WU(t)\boldsymbol{\omega}_{nb}^b \tag{62}$$

$$\dot{U}(t)\boldsymbol{\omega}_{nb}^b = \tfrac{1}{2}WU(t)\boldsymbol{\omega}_{nb}^b \tag{63}$$

By the definitions of $U(t)$ and W, the following equalities can be easily verified according to the unit-norm property of the quaternion $\boldsymbol{q}(t)$ and the definitions of $U(t)$ and W:

$$U(t)^TU(t) = I, \qquad U(t)^TWU(t) = -\left[\boldsymbol{\omega}_{nb}^b\times\right] \tag{64}$$

Multiplying $U(t)^T$ in Eq. (63) from the left and using Eq. (64), we obtain

$$U(t)^T\dot{U}(t)\boldsymbol{\omega}_{nb}^b = -\tfrac{1}{2}\boldsymbol{\omega}_{nb}^b\times\boldsymbol{\omega}_{nb}^b = \boldsymbol{0} \tag{65}$$

According to Eq. (64), Eq. (65), the definitions of the conventional equivalent tilt angle $\boldsymbol{\xi}(t)$, and the newly defined equivalent tilt angle $\tilde{\boldsymbol{\xi}}(t)$, the following relationship can be shown:

$$\begin{aligned}\tilde{\boldsymbol{\xi}}(t) &= \boldsymbol{\xi}(t) - 2\hat{U}(t)^T\left[\dot{\boldsymbol{q}}(t)\Delta + \tfrac{1}{2}\ddot{\boldsymbol{q}}(t)\Delta^2\right] \\ &= \boldsymbol{\xi}(t) - 2\{U(t) + \delta U(t)\}^T\left\{\tfrac{1}{2}U(t)\boldsymbol{\omega}_{nb}^b\Delta + \tfrac{1}{4}\dot{U}(t)\boldsymbol{\omega}_{nb}^b\Delta^2\right\} \\ &= \boldsymbol{\xi}(t) - \boldsymbol{\omega}_{nb}^b\Delta\end{aligned} \tag{66}$$

where the term δU^TU is neglected due to the normalization of the quaternion $\hat{\boldsymbol{q}}(t)$, the term $U(t)^T\dot{U}(t)\boldsymbol{\omega}_{nb}^b$ is neglected according to Eq. (65), and the term $\delta U^T\dot{U}\boldsymbol{\omega}_{nb}^b\Delta^2$ is neglected by Assumption 8. Combining Eqs. (33) and (66), we can establish a physical meaning of the newly defined equivalent tilt angle $\tilde{\boldsymbol{\xi}}(t)$ as follows:

$$C_{b(t-\Delta)}^{b'(t)} = I + [\tilde{\boldsymbol{\xi}}(t)\times] \tag{67}$$

where the $b(t-\Delta)$ frame is the true virtual body frame at the instant that the actual measurements are acquired.

Based on the definitions in Eqs. (23), (24), (55), and (57), inertial sensor biases satisfy the following simple relationship because they are modeled as constants:

$$\tilde{\nabla}(t) = \nabla(t) + \boldsymbol{b}_{\nabla} \tag{68}$$

$$\tilde{\varepsilon}(t) = \varepsilon(t) \tag{69}$$

From Eq. (58),

$$\dot{\delta\tilde{\boldsymbol{v}}} = \boldsymbol{\delta\dot{v}} + \ddot{\boldsymbol{v}}\Delta + \tfrac{1}{2}\dddot{\boldsymbol{v}}\,\Delta^2 \tag{70}$$

From Eq. (66), we obtain

$$\dot{\tilde{\boldsymbol{\xi}}} = \dot{\boldsymbol{\xi}} \tag{71}$$

and from Eqs. (28), (29), (68), and (69), it can be shown that

$$\dot{\tilde{\nabla}} = \dot{\nabla} = \boldsymbol{0} \tag{72}$$

$$\dot{\tilde{\varepsilon}} = \dot{\varepsilon} = \boldsymbol{0} \tag{73}$$

With the use of Eqs. (31), (55), (56), (58), and (66), the differential equation of the newly defined velocity error $\boldsymbol{\delta\tilde{v}}$ is expressed as follows:

$$\begin{aligned}
\dot{\delta\tilde{\boldsymbol{v}}} &= C(\boldsymbol{f}\times\boldsymbol{\xi}) - \boldsymbol{2\Omega}\times\left(\boldsymbol{\delta\tilde{v}} - \boldsymbol{\dot{v}}\Delta - \tfrac{1}{2}\ddot{\boldsymbol{v}}\Delta^2\right) + C\nabla + \ddot{\boldsymbol{v}}\Delta + \tfrac{1}{2}\dddot{\boldsymbol{v}}\,\Delta^2 \\
&= C(\boldsymbol{f}\times\tilde{\boldsymbol{\xi}}) - \boldsymbol{2\Omega}\times\boldsymbol{\delta\tilde{v}} + C\tilde{\nabla} - C\boldsymbol{b}_{\nabla} + (\boldsymbol{\Omega}\times\ddot{\boldsymbol{v}})\Delta^2 + \tfrac{1}{2}\dddot{\boldsymbol{v}}\,\Delta^2 \\
&\quad + C\left\{\boldsymbol{f}\times\boldsymbol{\omega}_{nb}^{b} + C^T\ddot{\boldsymbol{v}} + \boldsymbol{2}C^T(\boldsymbol{\Omega}\times\boldsymbol{\dot{v}})\right\}\Delta \\
&= C(\boldsymbol{f}\times\tilde{\boldsymbol{\xi}}) - \boldsymbol{2\Omega}\times\boldsymbol{\delta\tilde{v}} + C\tilde{\nabla} + C\dot{\boldsymbol{f}}\Delta + \tfrac{1}{2}C\ddot{\boldsymbol{f}}\Delta^2 \\
&\quad + C\left\{\boldsymbol{f}\times\boldsymbol{\omega}_{nb}^{b} + C^T\ddot{\boldsymbol{v}} + \boldsymbol{2}C^T(\boldsymbol{\Omega}\times\boldsymbol{\dot{v}}) - \dot{\boldsymbol{f}}\right\}\Delta
\end{aligned} \tag{74}$$

When Eqs. (7–9) and (46–48) are combined, the following equation is obtained:

$$\boldsymbol{f}\times\boldsymbol{\omega}_{nb}^{b} + C^T\ddot{\boldsymbol{v}} + \boldsymbol{2}C^T(\boldsymbol{\Omega}\times\boldsymbol{\dot{v}}) - \dot{\boldsymbol{f}} = \boldsymbol{0} \tag{75}$$

Substituting Eq. (70) and the definition of the equivalent accelerometer bias $\boldsymbol{b}_{\nabla}$ in Eq. (55) into Eq. (69), we obtain

$$\dot{\delta\tilde{\boldsymbol{v}}} = -\boldsymbol{2\Omega}\times\boldsymbol{\delta\tilde{v}} + C(\boldsymbol{f}\times\tilde{\boldsymbol{\xi}}) + C\tilde{\nabla} + \boldsymbol{d}_{\nabla} \tag{76}$$

$$\begin{aligned}
\boldsymbol{d}_{\nabla} &\equiv C\dot{\boldsymbol{f}}\Delta + \frac{1}{2}C\ddot{\boldsymbol{f}}\Delta^2 \\
&= \begin{bmatrix} 0 \\ 0 \\ 2v_m\omega_m\Omega_N\Delta\cos\theta(t) + v_m\omega_m^2\Omega_N\Delta^2\sin\theta(t) \end{bmatrix}
\end{aligned} \tag{77}$$

where $\boldsymbol{d}_{\nabla}$ indicates the equivalent accelerometer disturbance that is generated by the measurement delay Δ. When Eqs. (32) and (66) are combined, the attitude error equation expressed by $\dot{\tilde{\boldsymbol{\xi}}}$ is easily obtained as follows:

$$\begin{aligned}
\dot{\tilde{\boldsymbol{\xi}}} &= -\boldsymbol{\omega}_{ib}^{b}\times\boldsymbol{\xi} - \boldsymbol{\varepsilon} \\
&= -\boldsymbol{\omega}_{ib}^{b}\times\tilde{\boldsymbol{\xi}} - \boldsymbol{\varepsilon} - \left(\boldsymbol{\omega}_{ib}^{b}\times\boldsymbol{\omega}_{nb}^{b}\right)\Delta \\
&= -\boldsymbol{\omega}_{ib}^{b}\times\tilde{\boldsymbol{\xi}} - \boldsymbol{\varepsilon} - \left[\left(\boldsymbol{\omega}_{in}^{b} + \boldsymbol{\omega}_{nb}^{b}\right)\times\boldsymbol{\omega}_{nb}^{b}\right]\Delta \\
&= -\boldsymbol{\omega}_{ib}^{b}\times\tilde{\boldsymbol{\xi}} - \boldsymbol{\varepsilon} + \boldsymbol{d}_{\varepsilon}
\end{aligned} \tag{78}$$

$$\begin{aligned}
\boldsymbol{d}_{\varepsilon} &\equiv C^T\left(\boldsymbol{\omega}_{in}^{n}\times\boldsymbol{\omega}_{nb}^{n}\right)\Delta \\
&= [-\Omega_N\omega_m\Delta\sin\theta(t) \quad -\Omega_N\omega_m\Delta\cos\theta(t) \quad 0]^T
\end{aligned} \tag{79}$$

where $\boldsymbol{d}_{\varepsilon}$ indicates the equivalent gyro disturbance that is generated by the measurement delay Δ.

When Eqs. (72), (73), (76), and (78) (which together represent an error model corresponding to the past time that lags the current time by Δ), respectively, are compared with Eqs. (28), (29), (31), and (32) (which together represent an error model with respect to the current time), it can be observed that the two error models are identical except for the small equivalent inertial sensor disturbances $\boldsymbol{d}_{\nabla}$ and $\boldsymbol{d}_{\varepsilon}$ in Eqs. (77) and (79). As shown in Eqs. (76) and (78), the vertical velocity $\tilde{v}_D$, the roll error $\tilde{\xi}_x$, and the pitch error $\tilde{\xi}_y$ can be affected by the equivalent sensor disturbances $\boldsymbol{d}_{\nabla}$ and $\boldsymbol{d}_{\varepsilon}$. However, the vertical velocity $\tilde{v}_D$, the roll error $\tilde{\xi}_x$, and the pitch error $\tilde{\xi}_y$ are the states of good observability, and $\boldsymbol{d}_{\nabla}$ and $\boldsymbol{d}_{\varepsilon}$ are the trigonometric functions of the heading angle θ. The integration of a trigonometric function over one cycle is zero. In addition, both $\boldsymbol{d}_{\nabla}$ and $\boldsymbol{d}_{\varepsilon}$ have an attractive characteristic that they are proportional to the amount of measurement delay. Therefore, their effects can be gradually reduced if we identify and compensate for the measurement delay Δ.

IV. Heading and Accelerometer Bias Errors due to Measurement Delay

In the preceding sections, we derived steady-state conditions due to a measurement delay, and a new error model corresponding to immediate past time on a circular trajectory. When the steady-state condition of Eq. (49) is examined, it is concluded that both the sensitivity of the heading error and the driving term that is generated by the measurement delay are proportional to the magnitude of the velocity v_m.

The new error model composed of Eqs. (59), (72), (73), (76), and (78) indicates the convergence of the estimated navigation variables to the values at the immediate past time instead of the current time. In other words, the conventional GPS/SDINS Kalman filter does not account for the existence of the measurement delay Δ. The filter considers the GPS and the IMU measurements as if they were received at the same time. However, in reality, the GPS measurements lag the IMU measurements by the measurement delay time Δ. Thus, the output of the filter at the time t tends to converge to some neighborhood of the real value at the time $t-\Delta$.

As reported in Ref. 1, the ignorance of the measurement delay generates a large estimation error of the forward accelerometer bias. A large estimation error of the forward accelerometer bias in the calibration stage can cause large position and velocity errors in the navigation stage if no GPS measurements are available. A more detailed analysis on causes and effects of this phenomenon is possible if we utilize the results of the preceding sections. From the analysis, it can be shown that the measurement delay generates a bias in the heading error. The biased heading error, in turn, instantaneously accumulates a large error of the forward accelerometer bias.

To demonstrate and analyze the effect of the measurement delay in the GPS/SDINS Kalman filter, we performed a simulation representing an in-flight alignment. In the simulation, 12 error states consisting of $\boldsymbol{\delta v}$, $\boldsymbol{\xi}$, ∇, and ε were employed for the Kalman filter. The estimation errors were computed by comparing the true and estimated navigation variables as shown in Fig. 1. The trajectory segments used in the simulation are listed in Table 1. The trajectory is broken into four segments. Segments 1 and 4 are straight and level flight segments, whereas segments 2 and 3 are circular. Thus, they form an S-shaped trajectory. The forward speed is maintained at 10 π m/s throughout the trajectory segments. In the simulation, a gyro with a drift rate of 3 deg/h and an accelerometer with a random bias of 500 μg were used.

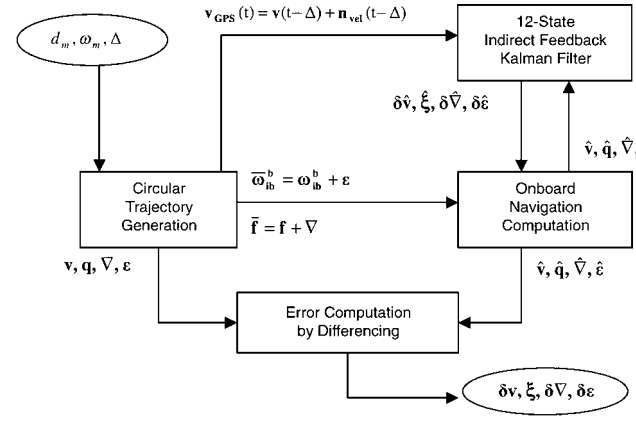

Fig. 1 Simulation configuration.

Table 1 Trajectory segments used in the simulation

Segment	Type	Duration, s	ω_m, deg/s
1	Straight	0–100	0
2	Circular	100–300	3.6
3	Circular	300–500	−3.6
4	Straight	500–600	0

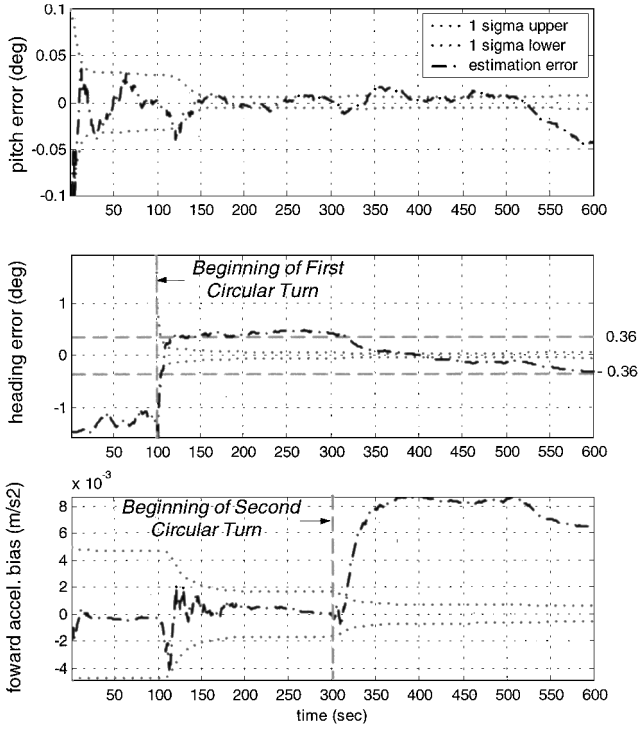

Fig. 2 Histories of pitch error, heading error, and forward accelerometer bias with GPS measurement delay of 0.1 s.

Figure 2 shows the time histories of the pitch, heading, and forward accelerometer bias estimation errors in the presence of the measurement delay of 0.1 s. Note that the estimation error of the forward accelerometer bias is related to both the pitch and heading errors as shown in Eq. (49). In Fig. 2, the dash–dotted lines indicate the estimation errors. They were computed by differencing the true and estimated navigation variables. The dotted lines indicate 1-sigma envelopes as computed by the Kalman filter. As can be seen in Fig. 2, the estimation error of the forward accelerometer bias becomes largest during segment 3. As can be seen by an abrupt decrease in the one-sigma envelop of the heading error in Fig. 2 during segment 2, the Kalman filter interprets the abrupt increase in the measurement residual of the forward velocity mainly due to the heading error. As a result, it can be observed in Fig. 2 that the heading error ξ_z approaches a value that equals the product of the heading angular rate and the measurement delay, namely,

$$\xi_z(t) \cong \omega_m \Delta \tag{80}$$

Note that $\omega_m \Delta = 0.36$ deg in the simulation. This result is consistent with the heading error model developed in Eq. (66). The pitch error ξ_y is very small compared to the heading error ξ_z. We can say that the measurement delay causes a large heading error but little pitch error, which agrees with Eq. (66). This is so because the angular rate vector $\boldsymbol{\omega}_{nb}^b$ has no roll and pitch elements as seen in Eq. (9).

During segment 3, a large estimation error in the forward accelerometer bias appears due to the measurement delay Δ. The large estimation error in forward accelerometer bias is, in fact, a direct consequence of the biased heading error during segment 2. As segment 3 begins, the sign of the heading angular rate ω_m is abruptly changed. Because of the sign reversal of the heading angular rate ω_m, the steady-state condition is changed from Eq. (81) to Eq. (82):

$$\nabla_x + v_m \omega_m \xi_z = v_m \omega_m^2 \Delta \tag{81}$$

$$\nabla_x - v_m \omega_m \xi_z = v_m \omega_m^2 \Delta \tag{82}$$

Note that the heading error ξ_z still approximately equals $\omega_m \Delta$ in the beginning of segment 3. Thus, as segment 3 begins, the Kalman filter drives the estimation of the forward accelerometer bias $\nabla_x(t)$ based on Eq. (82) as follows:

$$\nabla_x(t) \cong 2 v_m \omega_m^2 \Delta + v_m \omega_m [\xi_z(t) - \omega_m \Delta] \tag{83}$$

The term $\xi_z(t) - \omega_m \Delta$ in Eq. (83) is very small at the beginning of segment 3. As a consequence, the forward accelerometer bias $\nabla_x(t)$ instantaneously approaches the large value $2 v_m \omega_m^2 \Delta$ at the beginning of segment 3. To summarize, the biased heading error that is induced by the measurement delay Δ in the first circular turn is the key contributor that generates a large estimation error of the accelerometer bias in the remaining trajectory. A more detailed explanation for the error characteristics due to circular motion may be found in Ref. 7.

V. Calibration

A. Algorithm

In the preceding sections, the heading error was shown to be very sensitive to the measurement delay Δ. It was also shown that, on a circular trajectory, the heading error ξ_z approached the product of the heading angular rate ω_m and the measurement delay Δ if the maximum magnitude of the equivalent gyro disturbance $\boldsymbol{d}_\varepsilon$ was sufficiently small compared with the gyro bias ε as shown in Eq. (78). As shown in Eq. (49), the steady state of the heading error is not directly dependent on the gyro error. Thus, even in the case when the disturbance term $\boldsymbol{d}_\varepsilon$ is not negligibly small, the heading error would still approach $\omega_m \Delta$ if we initialize the error covariance matrix sufficiently large considering the effects of the measurement delay Δ as shown in Eq. (66) and adjust the noise strength of the roll and pitch gyros sufficiently large considering the effects of the measurement delay Δ as shown in Eq. (79).

Using the sensitivity of the heading error, a simple and efficient delay calibration algorithm is proposed. The key idea of the proposed calibration algorithm is to apply a trajectory in a controlled manner as an input to a GPS/SDINS Kalman filter. For the calibration, the vehicle is required to follow a trajectory consisting of two segments: a circular turn with a heading angular rate ω_1 beginning at t_1 and a circular turn with a heading angular rate ω_2 beginning at t_2. Before the beginning of the second circular turn, it is required to reset the GPS/SDINS Kalman filter to prevent a large accumulation of forward accelerometer bias. By the controlled maneuver, the amount of heading error change during the second circular turn would be near $(\omega_2 - \omega_1)\Delta$ if we drive the heading error near $\omega_1 \Delta$ during the first circular turn, which is possible because all of the error states of a GPS/SDINS Kalman filter are uniformly completely observable for circular trajectories.[8] The algorithm is summarized by the following equation:

$$\hat{\Delta} = \hat{\eta}_z / |\hat{\omega}_2 - \hat{\omega}_1| \tag{84}$$

In Eq. (84), $\hat{\omega}_1$ and $\hat{\omega}_2$ are the estimates of ω_1 and ω_2, respectively, and $\hat{\eta}_z$ is the accumulated heading error correction (AHEC) that is an estimation of the heading error change $(\omega_2 - \omega_1)\Delta$ during the second circular turn. If the residual azimuth gyroscope drift is zero and the position fixes are noise free, the difference between the AHEC $\hat{\eta}_z$ and the actual change of heading error $\xi_z(t_2) - \xi_z(t_1)$ would be zero. The AHEC $\hat{\eta}_z$ is an element of the accumulated attitude error correction vector $\hat{\boldsymbol{\eta}}(t, t_0) = [\hat{\eta}_x \;\; \hat{\eta}_y \;\; \hat{\eta}_z]^T$ that is computed from an output of the GPS/SDINS Kalman filter. Note that $\hat{\boldsymbol{\eta}}(t, t_0)$ should be reset to zero at the beginning of the second circular turn. During the propagation operation in the GPS/SDINS Kalman filter, the propagation of $\hat{\boldsymbol{\eta}}(t, t_0)$ is computed as follows:

$$\frac{\mathrm{d}}{\mathrm{d}t}\hat{\boldsymbol{\eta}}(t, t_0) = -\boldsymbol{\omega}_{ib}^b \times \hat{\boldsymbol{\eta}}(t, t_0) \tag{85}$$

Likewise, in parallel with the measurement update of the Kalman filter, $\hat{\boldsymbol{\eta}}(t, t_0)$ is updated as follows:

$$\hat{\boldsymbol{\eta}}(t, t_0) := \hat{\boldsymbol{\eta}}(t, t_0) + \boldsymbol{\delta}\hat{\boldsymbol{\xi}}(t) \tag{86}$$

where $\delta\hat{\boldsymbol{\xi}}(t)$ is an attitude error correction computed by GPS/SDINS Kalman filter.

Once the measurement delay is identified according to Eq. (84), the GPS position and velocity measurement inputs $\boldsymbol{v}_{\mathrm{GPS}}(t)$ and $\boldsymbol{r}_{\mathrm{GPS}}(t)$ should be corrected by a function of $\hat{\Delta}$ as follows:

$$\boldsymbol{v}_{\mathrm{GPS}}(t) := \boldsymbol{v}_{\mathrm{GPS}}(t) + \dot{\hat{\boldsymbol{v}}}(t)\hat{\Delta} + \tfrac{1}{2}\ddot{\hat{\boldsymbol{v}}}(t)\hat{\Delta}^2 \tag{87}$$

$$\boldsymbol{r}_{\mathrm{GPS}}(t) := \boldsymbol{r}_{\mathrm{GPS}}(t) + \hat{\boldsymbol{v}}(t)\hat{\Delta} + \tfrac{1}{2}\dot{\hat{\boldsymbol{v}}}(t)\hat{\Delta}^2 \tag{88}$$

where $\hat{\boldsymbol{v}}(t)$, $\dot{\hat{\boldsymbol{v}}}(t)$, and $\ddot{\hat{\boldsymbol{v}}}(t)$ are the velocity and its derivatives that are either retrieved or computed by the SDINS.

As compared with the existing methods, the calibration method proposed requires no hardware alteration. Thus, a rapid time synchronization of any combination of a GPS receiver and a strapdown IMU is possible. The software modification is also minimal because no expansion of the filter dimension is necessary.

If the heading angular rate and forward velocity are maintained constant, the calculation $\hat{\Delta}$ in Eq. (84) becomes simpler. $\hat{\Delta}$ is also constant, and it need not be recalculated in each measurement update afterward. Thus, the proposed algorithm can be used at the initial stage of real-time navigation to calibrate a constant measurement delay. The proposed method can also be used in an iterated manner with respect to the same set of data to reduce an error in calculating $\hat{\Delta}$.

B. Simulation

To evaluate the proposed algorithm, a simulation was performed. The setting of the simulation was the same as those used in Sec. IV, that is, a GPS was integrated with a medium to low grade SDINS. The integrated GPS/SDINS was flown to follow an S-shaped trajectory. In the simulation, the magnitude of the equivalent gyro disturbance $\boldsymbol{d}_\varepsilon$ in Eq. (79) is computed as

$$\|\boldsymbol{d}_\varepsilon\| \le \|\Omega_N \omega_m \Delta\| = \|12.0123(\mathrm{deg/h}) \times 0.0628(\mathrm{rad/s}) \times 0.1(\mathrm{s})\|$$

$$= 0.0754(\mathrm{deg/h}) \tag{89}$$

Because the magnitude of $\boldsymbol{d}_\varepsilon$ is much smaller than the 3 deg/h turn-to-turn repeatability error variance of the random gyro drift, its effect on the filter convergence can be ignored. Figure 3 shows the time histories of pitch, heading, and forward accelerometer bias estimation errors of the GPS/SDINS Kalman filter. In Fig. 3, the dotted lines indicate 1-sigma envelopes of the GPS/SDINS Kalman filter, the dash–dotted lines indicate the estimation errors of the filter without considering the measurement delay Δ, and the solid lines indicate the estimation errors after the proposed algorithm is applied. It is observed in Fig. 3 that the dashed lines are more or less within the dotted lines, that is, all of the heading, pitch, and forward accelerometer bias errors are within the corresponding 1-sigma envelopes. It can be concluded that the proposed algorithm efficiently identifies the measurement delay. The correction to the GPS/SDINS Kalman filter according to the identified measurement delay significantly reduces its heading, pitch, and forward accelerometer bias estimation errors. Note that the algorithm closely estimates a given 0.1 s of measurement delay.

In addition to the preceding result, various radii and heading angular rates were tested. A tendency was found that the calibration accuracy improves as the magnitude of $v_m \omega_m$ increases. If the heading angular rate is maximum during the controlled maneuver, the proposed algorithm would sufficiently eliminate the biased heading error and the undesirable large jump in the accelerometer bias during the entire trajectory. Another simulation result that compares the proposed algorithm with the conventional Kalman filter that is expanded by an error state representing the measurement delay Δ may be found in Ref. 9.

C. Experiment

In addition to the simulation, an experiment was carried out to confirm the proposed algorithm. A GPS/SDINS system consisting of the Sagem LP81 IMU with gyro drift of 3 deg/h and accelerometer bias of 500 μg and the NovAtel GPSCard was mounted on a test van, and an S-shaped trajectory was run. Because the error

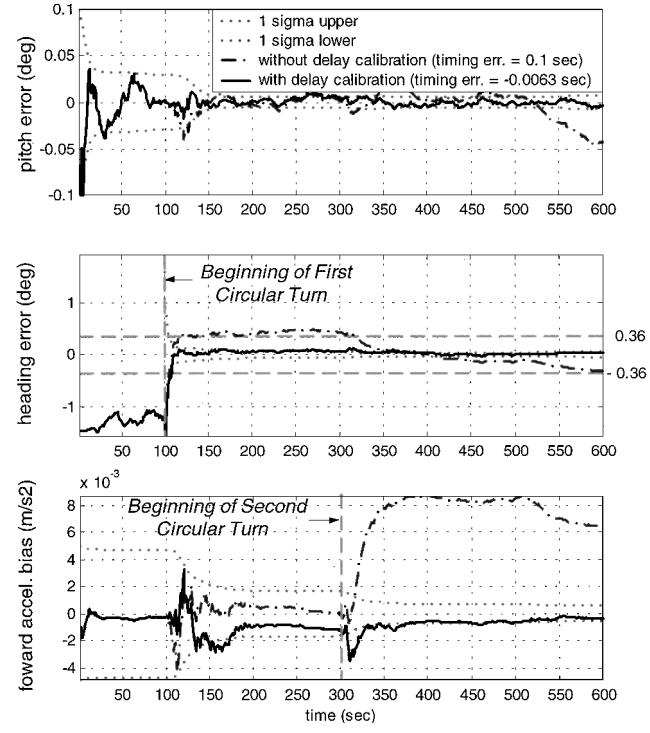

Fig. 3 Performance of the proposed calibration algorithm achieved in the simulation.

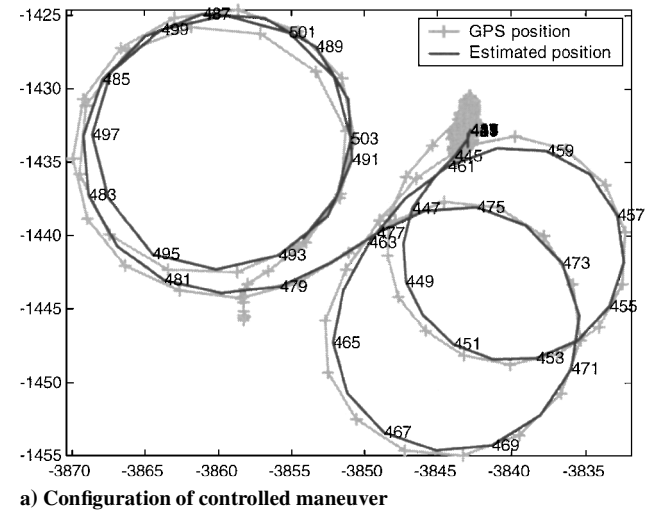

a) Configuration of controlled maneuver

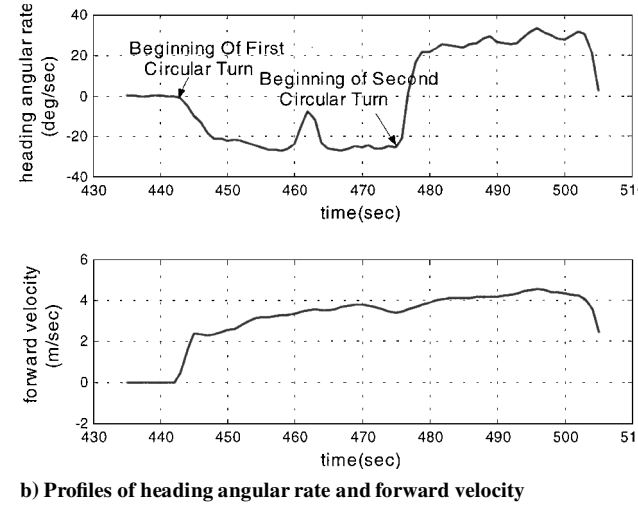

b) Profiles of heading angular rate and forward velocity

Fig. 4 Experimental trajectory.

sources of the IMU such as scale factor errors, misalignments, and mass unbalances are small compared with its constant random bias terms, Assumption 7 in Sec. II holds. All of the other assumptions are also generally satisfied. In the experiment, a 12-state velocity-aided Kalman filter is employed in an indirect feedback mode. The time interval between each measurement update of the Kalman filter was 1 s. The trajectory configuration is shown in Fig. 4a. The heading angular rate and the forward velocity profiles through the vehicle trajectory are shown in Fig. 4b. The average heading angular rate of the first and the second circular turns are −19.4 and 24.9 deg/s, respectively. The heading error variance is reset to 5 deg at the beginning of each circular turn. The variance of the GPS velocity measurements is set to 0.1 m/s. The test data are analyzed and shown in Fig. 5. In Fig. 5, the dotted lines indicate 1-sigma values computed by the GPS/SDINS Kalman filter, the dash–dotted lines indicate both the AHEC and estimated accelerometer bias without considering the GPS measurement delay, and the dashed lines indicate both AHEC and estimated accelerometer bias when applying the proposed algorithm. Because the difference between the AHEC and the actual heading error is constant if we assume no propagation noise, the history of the AHEC approximately depicts the tendency of the actual heading error during the second circular turn. As shown by the dash–dotted lines, the AHEC and the estimated forward accelerometer bias rapidly increase beginning from the second circular turn. By applying the calibration method of Eq. (84), we obtained an estimation of the measurement delay of 0.314 s. The true value of the measurement delay that was sought by the time-tagging method[2] was near 0.295 s. The solid lines in Fig. 5 are the results generated by the GPS/SDINS Kalman filter when the GPS measurements were compensated as in Eq. (87). When the dashed lines and the dotted lines of the 1-sigma values are compared, it can be concluded that the measurement delay is effectively calibrated in the experiment employing the proposed algorithm because the AHEC and the estimated forward accelerometer bias remain within the boundary of the variances of the heading error and the forward accelerometer bias throughout the trajectory.

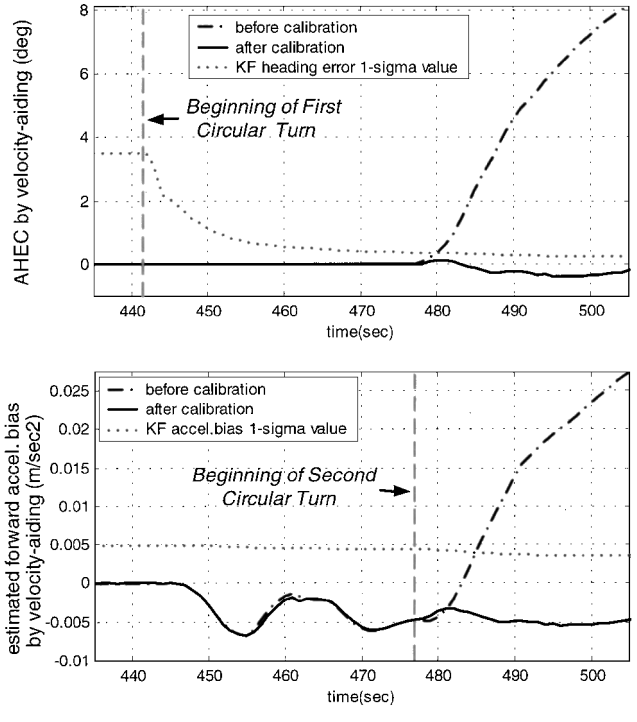

Fig. 5 Performance of the proposed calibration algorithm achieved in the experiment.

VI. Conclusions

In this study, we analyzed the effects of a constant transmission delay that occurs in delivering measurements from a GPS receiver to a Kalman filter for an aided SDINS. Steady-state conditions under the measurement delay are derived from the measurement residual observation. A new error model for the circular trajectories is derived, which shows that the currently computed navigation variables on circular trajectories converge not to the current true variables but to the neighborhood of the past true variables at the instant the delayed measurements were actually sampled. To reveal the causes and effects of the large estimation error of the accelerometer bias, an analysis is performed. It is shown that a biased heading error, together with an abrupt change of the steady-state condition, is the key element that stimulates a large estimation error of the forward accelerometer bias during S turns. Based on the steady-state conditions and the analysis results of the new error model, a simple delay calibration algorithm, based on the controlled vehicle maneuver, is proposed. Both the simulation and experiment results show that the proposed algorithm enables a simple and effective determination of the time synchronization of any combination of a GPS receiver and an SDINS. The important result of the analysis that the measurement delay drives the currently computed navigation variables not to the current true variables but to the neighborhood of the past true variables is also verified. Thus, it is recommended that the time synchronization between a GPS receiver and an SDINS should be achieved, at least, to the level where the product of the maximum heading angular rate and the measurement delay is small compared to the minimum heading error variance.

Acknowdegments

This work has been supported by the Automatic Control Research Center and Automation Systems Research Institute, Seoul National University, and by the Agency for Defence Development.

References

[1] Bar-Itzhack, I. Y., and Vitek, Y., "The Enigma of False Bias Detection in a Strapdown System During Transfer Alignment," *Journal of Guidance, Control, and Dynamics*, Vol. 8, No. 2, 1985, pp. 175–180.

[2] Knight, D., "Achieving Modularity with Tightly Coupled GPS/INS," *Proceedings of the IEEE PLANS '92*, Inst. of Electrical and Electronics Engineers, New York, 1992, pp. 426–432.

[3] Lee, H. K., Lee, J. G., Roh, Y. K., and Park, C. G., "Modeling Quaternion Errors in SDINS: Computer Frame Approach," *IEEE Transactions on Aerospace and Electronic Systems*, Vol. 34, No. 1, 1998, pp. 289–299.

[4] Benson, D. O., Jr., "A Comparison of Two Approaches to Pure-Inertial and Doppler-Inertial Error Analysis," *IEEE Transactions on Aerospace and Electronic Systems*, Vol. 7, No. 4, 1975, pp. 447–455.

[5] Weinreb, A., and Bar-Itzhack, I. Y., "The Psi-Angle Error Equation in Strapdown Inertial Navigation Systems," *IEEE Transactions on Aerospace and Electronic Systems*, Vol. 14, No. 3, 1978, pp. 539–542.

[6] Bar-Itzhack, I. Y., "Modeling of Certain Strapdown Heading-Sensitive Errors in INS Error Models," *Journal of Guidance, Control, and Dynamics*, Vol. 8, No. 1, 1985, pp. 142–144.

[7] Lee, H. K., Lee, J. G., and Jee, G. I., "Effect of GPS Measurement Delay on SDINS," *Proceedings of the IEEE PLANS 2000*, Inst. of Electrical and Electronics Engineers, New York, 2000, pp. 464–471.

[8] Goshen-Meskin, D., and Bar-Itzhack, I. Y., "Observability Analysis of Piece-Wise Constant Systems, Part II: Application to Inertial Navigation In-Flight Alignment," *IEEE Transactions on Aerospace and Electronic Systems*, Vol. 28, No. 4, 1992, pp. 1068–1075.

[9] Lee, H. K., Lee, J. G., and Jee, G. I., "Calibration of Time Synchronization Error in GPS/SDINS," *Proceedings of the 15th IFAC Symposium on Automatic Control in Aerospace*, Elsevier Science, Oxford, England, U.K., 2001, pp. 223–228.